Chemical Physics Letters 495 (2010) 102–108

Contents lists available at ScienceDirect

Chemical Physics Letters

journal homepage: www.elsevier.com/locate/cplett

Negative-electron-affinity diamondoid monolayers as high-brilliance source for ultrashort electron pulses

S. Roth [a], D. Leuenberger [a], J. Osterwalder [a], J.E. Dahl [b,1], R.M.K. Carlson [b], B.A. Tkachenko [c], A.A. Fokin [c,2], P.R. Schreiner [c], M. Hengsberger [a,*]

[a] Physik-Institut der Universität Zürich, Winterthurerstrasse 190, CH-8057 Zürich, Switzerland
[b] MolecularDiamond Technologies, Chevron Technology Ventures, 100 Chevron Way, Richmond, CA 94802, USA
[c] Institut für Organische Chemie, Justus-Liebig-Universität Giessen, Heinrich-Buff-Ring 58, D-35392 Giessen, Germany

ARTICLE INFO

Article history:
Received 3 February 2010
In final form 21 June 2010
Available online 25 June 2010

ABSTRACT

Diamondoids are nanometer-sized, hydrogen terminated diamond-like molecules consisting of fused adamantane units. The thiolated diamondoid [121]tetramantane-6-thiol shows negative electron affinity behavior, *i.e.* population of unoccupied states directly leads to spontaneous electron emission. We present time-resolved photoemission data from self-assembled monolayers of [121]tetramantane-6-thiol in order to shed light on the emission process: A photon energy threshold for electron emission of 5.6–5.8 eV was observed, and the electron affinity was estimated to be −0.21 to −0.57 eV for Ag and Au substrates, respectively. Electrons are emitted after excitation in the metal substrate through the molecular orbitals within a few femtoseconds.

1. Introduction

Molecular layers on surfaces are one of the most promising routes toward the miniaturization of devices to nanometer dimensions [1]. Diamondoid molecules are potential candidates for a large variety of applications, where functionalized nanometer-sized building blocks are required [2]. While it is known since 1933 that diamondoids occur with small abundance in crude oil [3], the interest in diamondoids was fueled only recently by the successful isolation of larger amounts of higher diamondoids from natural gas condensates [4] and their facile C–H-bond functionalization [5]. Diamondoids constitute a quite special class of alkanes because they display the cubic diamond carbon framework and because of their peculiar properties. Starting from the smallest diamondoid, adamantane, with the formula $C_{10}H_{16}$, the next higher diamondoids can be constructed by adding C_4 alkyl units, at least up to hexamantanes, from where on cyclic diamondoids can be constructed in several ways from lower diamondoids [6]. The first member of the series of higher diamondoids is tetramantane, $C_{22}H_{28}$, which is the first diamondoid that exists in isomeric forms. It can be synthesized [7], but can be isolated in sizable amounts only from crude oil [4].

Due to the negative electron affinity (NEA) behavior of hydrogen-terminated bulk diamond [8–12] and nano-structured diamond grown by chemical vapor deposition [13,14] it was anticipated that this might be the case for diamondoid thin films as well [15]. Monolayer films can be prepared on noble metal surfaces by replacing hydrogen by a thiol group using the latter as a linker to the metallic substrate [16]. In this way, molecular layers can be produced in excellent quality on Ag(111) and Au(111) surfaces in solution due to self-assembly, necessitating only minor follow-up treatment inside the vacuum system [17,18]. [121]tetramantane corresponds to the elongated C_{2h}-isomer, whose structure corresponds to four diamond cages aligned along the bulk diamond [100]-direction (see Fig. 1). According to X-ray absorption measurements, the [121]tetramantane-6-thiol molecules adsorb in upright orientation on the surfaces, the sulfur-carbon bond including an angle of about 30° with the surface normal [17]. From such self-assembled monolayers (SAM) of [121]tetramantane-6-thiol, NEA behavior was demonstrated by means of photoemission experiments at a synchrotron light source [18,19].

Molecules of [121]tetramantane in flat arrangement on gold have been investigated by scanning tunneling microscopy and spectroscopy [20], and the results were compared with density functional computations [20–22]. From these measurements and computations, the energy gap between the highest occupied and the lowest unoccupied molecular orbitals (HOMO and LUMO, respectively) of tetramantane was estimated to be much larger

* Corresponding author. Fax: +41 44 635 5704.
E-mail address: matthias.hengsberger@physik.uzh.ch (M. Hengsberger).
[1] Present address: Geballe Laboratory for Advanced Materials, Stanford University, Stanford, CA 94305, USA.
[2] Address: Department of Organic Chemistry, Kiev Polytechnic Institute, 03056 Kiev, Ukraine.

0009-2614/$ - see front matter © 2010 Elsevier B.V. All rights reserved.
doi:10.1016/j.cplett.2010.06.063

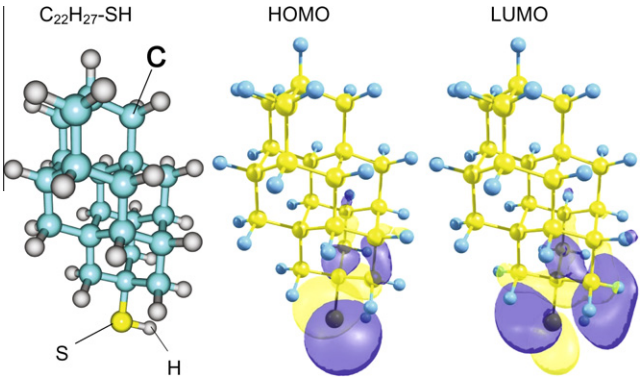

Fig. 1. Molecular orbitals of [121]tetramantane-6-thiol. Ball-and-sticks model of the [121]tetramantane-6-thiol-molecule terminated by hydrogen (left panel) and highest occupied (center panel, HOMO) and lowest unoccupied (right panel, LUMO) molecular orbitals. The atom positions are superimposed for the sake of clarity.

than 5 eV and the electron affinity to be about −0.3 eV, in agreement with previous density functional and quantum Monte Carlo computations [15]. These findings suggest that NEA is an intrinsic property of diamondoid molecules. However, relevant properties like the energy gap of diamondoids, the electronic states involved in the excitation, as well as the properties at low photon frequencies, which would be important for applications, could not be fully resolved.

In order to elucidate the properties and excitation mechanisms of these molecular layers, we carried out time-resolved photoemission experiments on layers of [121]tetramantane-6-thiol deposited from solution onto the noble metal surfaces Ag(1 1 1) and Au(1 1 1).

2. Experiment

The [121]tetramantane powder had been obtained by isolation from natural gas condensates and subsequent purification by liquid chromatography [4]. The diamondoid was monohydroxylated [23] and thiolated to yield [121]tetramantane-6-thiol [16]. [121]Tetramantane-6-thiol was deposited according to the recipe given in Ref. [18]. Briefly, after careful *in situ* preparation of the Ag(1 1 1) and Au(1 1 1) surfaces using standard routines of Ar–ion sputtering and annealing, the sample surfaces were immersed *ex situ* into 1–10 mM [121]tetramantane-6-thiol solution for about 24 h in a closed vial. After deposition, the samples were removed from the solution, rinsed with ethanol, dried with nitrogen and inserted into the load lock of the vacuum system within one minute. The surfaces were found to be stable over a few days in vacuum at a base pressure in the 10^{-11} mbar range. By means of X-ray photoelectron spectroscopy the coverage and the binding energy of the sulfur $2p_{3/2}$ core level were checked. The latter exhibits the typical chemical shift of an intact thiol bond between a metal substrate and an organic molecule [17,24]. The saturation coverage as measured by X-ray photoemission, and referred to hereafter as monolayer, was 1 molecule per 3.2 ± 0.24 Ag atoms, which is compatible with the well-known saturation $\sqrt{3}\times\sqrt{3}R30^\circ$ reconstruction of thiol compounds in high-density packing on noble metal surfaces [25,26].

The sample stability was checked by exposing the samples repeatedly to intense radiation from the laser over long periods of time and by taking spectra between two subsequent intervals. Surprisingly, it was found that the sample quality, as characterized by the strength of the NEA peak, was *improved*. The efficiency of this optical annealing saturates when the integrated charge reaches a value corresponding to a few thousand electrons per molecule.

The photoemission setup consists of a laser oscillator providing 55 fs pulses with a central wavelength of 800 nm [27], a regenerative amplifier (repetition rate 100–250 kHz), and a widely tunable optical parametric amplifier [28]. From cross-correlation experiments, pulse widths of 94 and 105 fs are inferred for fundamental and second harmonic light at the sample position, respectively. The light was *p*-polarized with an angle of incidence of 30° with respect to the surface normal. The photoelectron spectra were acquired using a modified VG ESCALab system [29]. In order to avoid the low transmission of the electron analyzer at very low kinetic energies, the sample was biased to −10 V. The total photoelectron yield was measured as drain current to ground by means of a Keithley 485 pico-ammeter. All data were taken at room temperature.

3. DFT computations

In order to determine the orbitals spanning the energy gap in the case of the thiolated compound, we performed density functional computations using the Gaussian 03 program suite as described in Ref. [22]. The B3PW91 exchange–correlation functionals and the cc-pVDZ basis set were used. The shapes of the HOMO and LUMO are presented in Fig. 1 next to a ball-and-sticks model of the molecule. The charge density of both states is located at the sulfur atom in contrast to HOMO and LUMO of the bare diamondoid [22]. For the energy gaps, we obtain 6.9 eV for the HOMO–LUMO gap of [121]tetramantane-6-thiol in gas phase and 8.14 eV for the energy gap between HOMO − 1 and LUMO + 1, which is close to the value of the true HOMO–LUMO gap of the bare diamondoid. We want to point out that these values are likely to be changed by absorption onto the substrate [22] or in a high-density package, as in a crystal (see discussion in Ref. [30]).

4. Negative electron affinity

Photoemission spectra taken from a tetramantane-SAM on Ag(1 1 1) are presented in Fig. 2a and compared to a spectrum from pristine Ag(1 1 1). Furthermore, two-photon-photoemission (2PPE) spectra taken with 3 eV photons are shown in Fig. 2b. Common to all these spectra taken from the tetramantane-SAM sample is the sharp and strong peak at 4.43 eV at the low-energy cut-off of the spectra, with a full-width-at-half-maximum (FWHM) of 0.15 eV in the 2PPE spectra. The peak position and the peak width scatter between different sample preparations by about ±0.1 eV and ±0.015 eV, respectively.

It is interpreted as emission from the LUMO, which is located above the vacuum level, the tetramantane-SAM thereby acting as an electron emitter with negative electron affinity (NEA) [18]. In fact, for the low-energy spectra, about 80% of the total spectral weight is emitted within the NEA peak due to the fact that many highly excited electrons are transferred to the molecule during thermalization and accumulate at the conduction band bottom, *i.e.* the LUMO. In contrast, photoemission intensity from the substrate is completely suppressed in presence of the 1 nm thick layer owing to the short escape depth of low-energy electrons from solids. The high-energy cut-off of the vuv-spectrum displayed in Fig. 2a is given by the valence band maximum of the tetramantane-SAM, *i.e.* the HOMO. From the high-energy edge of the HOMO and the position of the LUMO, the HOMO–LUMO gap of [121]tetramantane-6-thiol is estimated to be $5.7^{+0.2}_{-0}$ eV, which is to be compared to the value of 6.9 eV obtained from the density-functional computations. It has to be emphasized that the actual HOMO–LUMO gap of the diamondoid moiety is much larger, and slightly increasing from 8.05 to 8.14 eV upon addition of the thiol group (Ref. [22] and this work). In contrast, the gap of [121]tetramantane-6-thiol is determined by the orbital energies of the sulfur lone

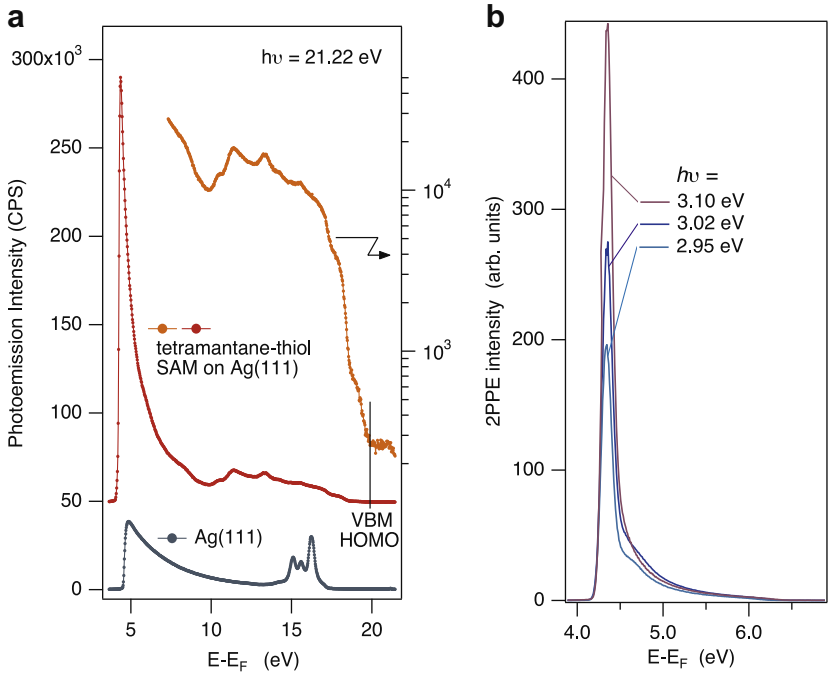

Fig. 2. Photoemission from [121]tetramantane-6-thiol/Ag(111). (a) Valence band spectra using vuv-photons of 21.22 eV plotted against the final state energy with respect to the Fermi energy. Spectra of pristine Ag(111) (blue, bottom curve) and tetramantane-SAM (top, red and orange curves) are shown. The latter is shown twice, once against the right logarithmic axis (orange, uppermost curve). The spectra are offset vertically for the sake of clarity. The assumed valence band maximum (VBM) is indicated by a vertical line. (b) Two-photon photoemission spectra taken with selected photon energies. (For interpretation of the references to colour in this figure legend, the reader is referred to the web version of this article.)

pair electrons, and hence in our case by the covalent bond formed between the metal substrate and the sulfur group, as displayed in Fig. 1.

The low-energy cut-off of photoemission spectra usually is determined by the position of the vacuum level, allowing the workfunction of the sample to be calculated. In our case, however, no electrons are observed at energies below the NEA peak position. One possibility to get an absolute value of the electron affinity is to estimate the position of the vacuum energy by computing the change in surface dipole moment due to charge transfer between the metal substrate and the sulfur group of the molecule. Such values have been computed for thiolated alkane layers adsorbed onto noble metals [31]. Assuming the density of molecules obtained from core-level photoemission experiments the shift in work function can be estimated to be −0.55 eV and −1.48 eV for the case of Ag and Au, respectively. Taking the workfunctions of the pristine surfaces (4.74 eV and 5.31 eV for Ag and Au, respectively) into account, we arrive at an electron affinity of −0.21 eV for tetramantane-SAM/Ag(111) and of −0.57 eV for tetramantane-SAM/Au(111).

5. Excitation pathway

As can be seen from Fig. 2b, the intensity of the NEA peak depends strongly on photon energy. In fact, more extended measurements through the whole visible light range reveal a threshold behavior as shown by plotting the integrated yield of photoelectrons from the NEA peak versus the photon energy (Fig. 3). The data have been carefully normalized for photon flux and pulse width by simultaneously recording the photocurrent from a polycrystalline Ag sample. Moreover, from fluence-dependent measurements, displayed in the inset in Fig. 3, it can be concluded that the excitation occurs via two-photon ionization [32]. Therefore, at the threshold, total photon energies of 5.56 ± 0.04 eV and

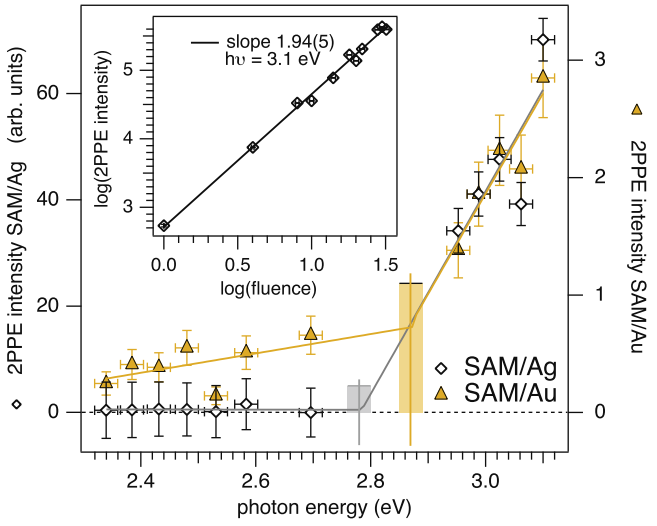

Fig. 3. Photon energy dependence of the NEA peak intensity in 2PPE spectra. The intensity was integrated over an energy window of about 200 meV. Data obtained for a tetramantane-SAM deposited on Ag(111) and Au(111) are shown as grey open and yellow solid symbols against the left and right axis, respectively. The extrapolated photon energy thresholds are marked by rectangles for both cases, the widths of which denote the uncertainty. Inset: the 2PPE intensity as measured by using 3.1 eV photons is shown as function of fluence in a logarithmic plot. The curve has a slope of 2, indicating a second order, *i.e.* two-photon process.

5.74 ± 0.04 eV are to be provided for exciting electrons into the LUMO in the case of Ag and Au substrates, respectively.

Looking at the valence band structure of the substrate, the threshold can be attributed to the minimum photon energy of a direct two-photon transition, necessary to promote an electron from the occupied Ag-*sp* band into a final state at the same or a higher energy than the LUMO. This situation is depicted in Fig. 4 by the

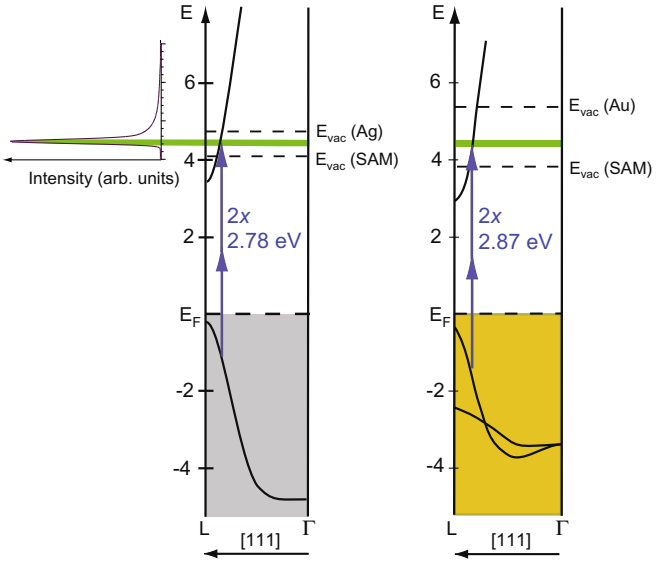

Fig. 4. Threshold transition in the substrate bandstructure. In the left and right panel, the bulk bandstructures are displayed along the [1 1 1]-direction in silver and gold, respectively [33]. The threshold transitions into the LUMO (green line) are indicated by blue double arrows. The calculated positions of the vacuum level are plotted as horizontal dashed lines for the bare metal surfaces and the [121]tetramantane-6-thiol-SAM. (For interpretation of the references to colour in this figure legend, the reader is referred to the web version of this article.)

double arrow indicating the corresponding momentum of the direct two-photon transition along the Λ-line in the respective band structure [33]. Thus, the excitation is likely to occur in the metal substrate as suggested by Yang et al. [18].

Clear evidence for this model can be obtained by taking advantage of the inherent time-resolution of the two-photon experiment: in case of direct transitions across the diamondoid gap, the two photons need to be absorbed simultaneously, whereas in case of a two-step excitation involving real states in the metal, the intensity of the transition is expected to decay exponentially due to the finite lifetime of the populated intermediate state. The results of the time-resolved measurements are shown in Fig. 5a. The intensity is clearly asymmetric towards positive delays indicating a population decay with fairly long time constants. Moreover, the fact that the decay times decrease with increasing energy is strongly reminiscent of a metallic band, where the phase space available for scattering events increases roughly quadratically with energy [34–36].

In order to confirm our interpretation, we compared the decay times extracted by fitting the experimental data using rate equations with results obtained from a numerical simulation. The latter was performed using a model similar to the one used in Ref. [37], including cascade-like relaxation processes and multi-photon excitations explicitly, and transport effects phenomenologically through an effective lifetime [34]. The lowest-order process is depicted in Fig. 5b, the results are shown in panels Fig. 5c–e: the range of decay times obtained from the simulations for various lifetime and transport models are found to be in good agreement with our measurements. Nevertheless, the measured cross-correlation curve obtained from the NEA peak cannot be fully reproduced in the simulations because the rising edge at negative delays is steeper in the measurements than the experimental, bare pulse cross-correlation curve the calculations were based on. The steep rising edge can be rationalized, however, by allowing electrons to be excited directly into the LUMO by simultaneous absorption of two pump photons and one probe photon. The cross-correlation width of this three-photon-process should be 124 fs as compared to 141 fs of the two-photon process. The transients of the NEA peak were fitted by the sum of direct transitions (40 ± 3%) and contributions from the hot electron gas (60 ± 3%) in the substrate. The results are shown in Fig. 5c together with the relative contributions. The whole hot electron dynamics output by the calculations are displayed on a logarithmic color scale in Fig. 5e. One can clearly distinguish various multi-photon processes with distinct delay dependence, and processes involving either only pump or only probe photons which show no dependence (bleaching of initially occupied states can be neglected at the fluences and excitations densities used here).

Taking these results together, we may conclude that the main excitation channel is provided by the metal substrate.

6. Electron emission process

In order to measure the overall duration of the excitation and emission process, several attempts were made to clock the precise moment of electron emission from the LUMO. One method takes advantage of the direct interaction of the electron with a probing light field after emission. If an ultrashort probing light pulse arrives at the sample at the moment of electron emission, the electron is accelerated in the electric field. As a consequence, the photoemission spectrum may be changed by the appearance of sidebands due to the direct interaction between the emitted electron and the electric field [38,39]. The sidebands appear only if the temporal uncertainty of the process under investigation is longer than the period of one optical cycle of the light wave [38]. Under this condition, the spacing of these sidebands equals the photon energy of the probing light field. Two selected spectra are shown in Fig. 6a: the spectrum for negative delay corresponds to the spectrum obtained without red pulse. In coincidence, the intensity of the NEA increases due to additionally available electrons above the Fermi level, and additional spectral weight is observed between the NEA peak and $E - E_F = 4.65$ eV, which corresponds to electrons excited from the Fermi level by absorption of one blue (3.1 eV) and one red (1.55 eV) photon. This signal can be used to measure the cross-correlation function of the light pulses and to determine the precise zero delay. No sidebands were observed in our datasets taken at various probe photon energies, which suggests that the timescale of the electron emission process is faster than 2.7 fs, which is the temporal period of 800 nm light.

After emission the electron feels the electric field of the pulse during its drift to the detector. Integrated over the time the light field acts on the electron, the positive and negative accelerations partially cancel and result in a broadening of the peak shape. The effect observed being quite small, several methods were used for the determination of the peak width. In order to be independent of the precise lineshape of the NEA peak, we calculated the root-mean-square deviation from the spectral center of gravity, referred to hereafter as r.m.s. width, as function of delay in Fig. 6b. Indeed, a small broadening of $\gtrsim 2$ meV could be observed close to delay zero. Note that any finite delay of electron emission should result in a shift of the correlation maximum to negative delays in the representation of Fig. 6b. Despite the smallness of the additional broadening, the effect is too large to be explained by space-charge effects owing to the increase in electron yield around time delay zero [40,41]. Even in this case, however, space-charge effects would yield the same results because the broadening of the electrons within the NEA peak almost exactly occurs at delay zero, which means that the electrons emitted through the LUMO leave the sample without significant time delay.

From all these considerations, we may therefore conclude that the retention time of the electron in the LUMO be of the order of a few femtoseconds. This result can be compared to results of a

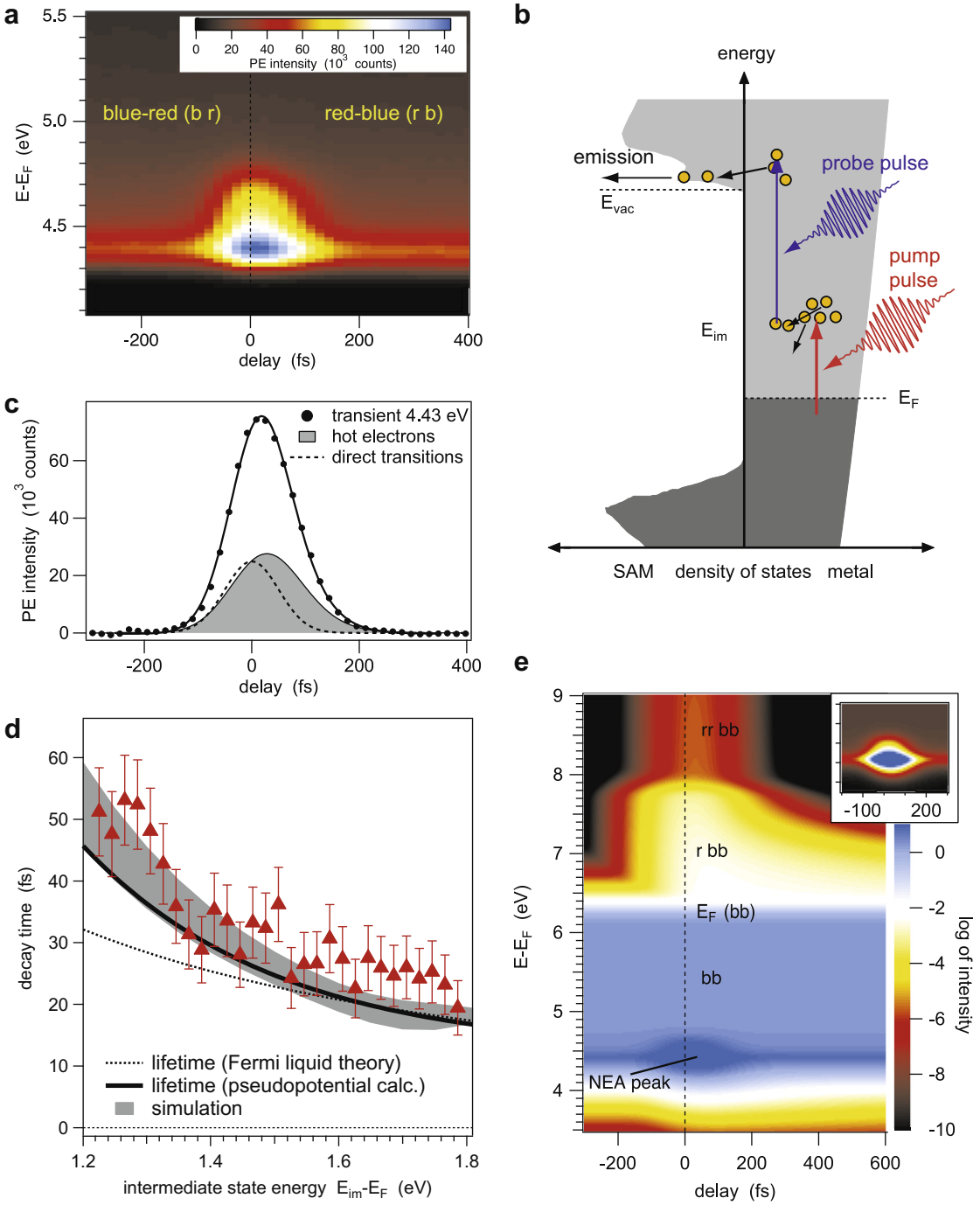

Fig. 5. Time-resolved photoemission data from tetramantane-SAM/Ag(1 1 1) for low pulse energy. (a) 2PPE intensity color-coded and plotted versus time delay (*x*-axis) and electron energy (*y*-axis) for the tetramantane-SAM/Ag sample. At zero delay, both pump ($h\nu$ = 1.55 eV, red) and probe (3.1 eV, blue) pulse arrive at the same time; the photon sequence for positive and negative delays is indicated. (b) Model used for the numerical simulations showing only the lowest order process: electrons are excited by a pump pulse (red) to intermediate state energies E_{im} above the Fermi level, from where they start to thermalize; a delayed probe pulse (blue) excites remaining electrons into states above the LUMO energy, from where they relax and finally are emitted. (c) Transient at constant-energy at the peak maximum (solid circles) and fit to the data (solid line) together with the relative contributions of direct transitions (dashed line) and hot carriers (grey shaded area). The constant background was subtracted in all cases. (d) Decay times of the intermediate states excited by the pump pulse as obtained by fitting rate equations to cross-correlation curves as function of electron energy. The black curves give the bare lifetimes of excited states in Ag, computed within two different theoretical models, *i.e.* modified Fermi liquid theory [35] (dashed line) and a pseudopotential plane-wave calculation [36] (solid line). The grey shaded area corresponds to the decay times resulting from the numerical simulations including the uncertainty due to different lifetime models. (e) Result of the numerical simulations in logarithmic color code in order to enhance the higher-order processes indicated by the photon sequence (r $h\nu$ = 1.55 eV, b $h\nu$ = 3.1 eV). Inset: idem for the NEA peak on a linear color scale. The lineshape was approximated by using a lorentzian multiplied with a step function at the low-energy cut-off. (For interpretation of the references to colour in this figure legend, the reader is referred to the web version of this article.)

2PPE study on Ar layers of variable thickness adsorbed onto Cu(001) [42]. Argon is known to exhibit negative electron affinity. Electrons excited in the substrate above the vacuum level but still below the conduction band of the Ar layer are trapped between the substrate and the Ar layer. The retention time of the electrons in this trapped state depends on the attempt rate of the electrons trying to tunnel through the layer and on the thickness of the layer. The attempt frequency was determined to be 1/1.4 fs^{-1} and no sig-

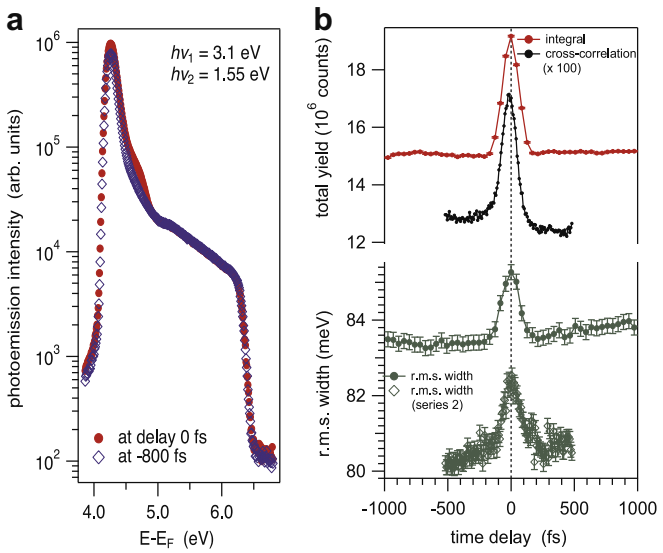

Fig. 6. Time-resolved data from tetramantane-thiol on Ag(1 1 1). (a) 2PPE spectra from diamondoid SAM were recorded using a photon energy of 3.1 eV (above threshold) as function of time delay with respect to an intense red pulse (1.55 eV, absorbed fluence 60 μJ/cm^2 [32]). Two selected spectra are shown in the left panel for time delay zero and for a large negative delay. (b) From the top to the bottom: integral yield (red dots), cross-correlation curve (black dots), and root-mean-square (r.m.s.) width (solid and open green diamonds for two selected measurements) of the NEA peak. The error bars indicate the statistical uncertainty of the data. (For interpretation of the references to colour in this figure legend, the reader is referred to the web version of this article.)

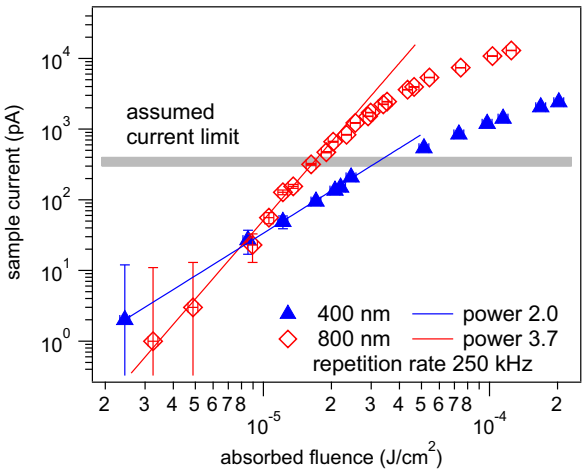

Fig. 7. Total photoelectron yield as function of absorbed fluence [32]. The total yield, measured as photocurrent, is shown for excitation with 400 nm (solid blue triangles) and 800 nm light (red open diamonds). The lines are guides to the eye; their slopes (fitted power laws) indicate the order of the multi-photon process. The grey shaded area denotes the photoelectron yield where the current starts to deviate from the expected power law. (For interpretation of the references to colour in this figure legend, the reader is referred to the web version of this article.)

nificant increase in retention time was observed for a layer thickness of 10 Å [42], which corresponds to the size of the carbon cage of [121]tetramantane-6-thiol. Assuming a similar attempt frequency for electrons in the LUMO of [121]tetramantane-6-thiol, we obtain an upper bound of a few femtoseconds for the total duration of the emission process, in good agreement with the present observations.

From the ultrashort transit time of the electrons through the LUMO, one may infer that this kind of emitter would be suitable for applications requiring a high current density. In fact, a long lifetime of the electrons in the LUMO would lead to an accumulation of electrons and thereby to a Coulomb blockade in the molecule, decreasing the efficiency of the charge transfer between substrate and molecules. In order to measure the critical current density, the total yield of photoelectrons was recorded as a function of absorbed light fluence. The result is shown in Fig. 7 on a logarithmic scale for two photon energies. In this plot the photocurrent increases with the second and forth power of the fluence for photons of 3.1 eV (400 nm) and 1.55 eV (800 nm), respectively. For currents exceeding the absolute value of 320 pA or corresponding current densities higher than 4 μA/cm^2, the current deviates from the extrapolated power law. The critical current density corresponds to about 210 A/cm^2 in continuous mode or else to 0.1 electrons per second per molecule. The inverse of this rate is much larger than the lifetime of the excited LUMO state. Therefore, we may safely conclude in view of potential applications that the current density of such NEA emitters is limited solely by repulsive forces between emitted electrons outside the emitting surface.

Very recently, the relative quantum efficiency of photoemission from [121]tetramantane-6-thiol on gold with respect to that of pristine gold was determined from soft X-ray photoemission data and Monte Carlo simulations to be of the order of 1.3 [19]. Comparing our data taken from [121]tetramantane-6-thiol/Ag(1 1 1) and pristine silver, we find a factor of about 2.2, confirming the observation of a strong increase of the quantum efficiency due to the presence of the diamondoid layer. The critical current density (Fig. 7) can be converted in an absolute quantum efficiency of 2×10^{-6} electrons per absorbed photon. From these numbers and a comparison with absolute yield measurements from Au [43] one may expect an absolute yield of 5×10^{-4} at a photon energy of 6 eV. In view of an application as photocathode, we anticipate that its properties currently are limited by the space charge in vacuum like in any other cathode material whilst offering a highly monochromatic spectrum and an excellent time structure and a high stability over long periods of time. The best compromise between minimizing the high-energy tail of the spectrum and enhancing the quantum efficiency must be found by tuning the photon energy in order to achieve truly high brilliance.

7. Summary

In conclusion, our measurements shed new light on the negative electron affinity behavior of [121]tetramantane-6-thiol monolayers on Ag and Au surfaces. The electron affinity could be estimated to be −0.21 eV (−0.57 eV) for Ag(Au) substrates, and the HOMO–LUMO gap of the thiolated diamondoids could be estimated to be of the order of 5.7 eV. As already conjectured in previous publications [18,19], the excitation occurs in the metal. Moreover, a very efficient charge transfer mechanism allows the electron to be promoted into the diamondoid LUMO, from where it is emitted instantaneously with an upper bound of a few femtoseconds. Moreover, the fact that the photoelectron yield is reasonably high for the fundamental and harmonics of Ti:sapphire lasers, and that the tetramantane-SAM can easily be mass produced in solution, makes [121]tetramantane-6-thiol layers very promising candidates for use as photocathodes. Due to the fast excitation channel and the short retention time of the electrons in the LUMO, ultrashort electron bunches of a few femtoseconds duration may routinely be produced by excitation with a suitable pulsed light source.

Acknowledgement

We gratefully acknowledge W. Yang, Z. Liu and J. Fabbri for their valuable help in preparing the samples, and Z.-X. Shen for valuable

discussions as well as for initiating the collaboration. We acknowledge the help of A. Devizis during some of the experiments and O. Steinkamp for helping in the statistical analysis. This work has been supported by the Swiss National Science Foundation and by the Deutsche Forschungsgemeinschaft.

References

[1] J.V. Barth, G. Constantini, K. Kern, Nature 437 (2005) 671.
[2] P.R. Schreiner et al., J. Org. Chem. 71 (2006) 6709.
[3] S. Landa, V. Macháček, Coll. Czech. Chem. Commun. 5 (1933) 1.
[4] J.E. Dahl, S.G. Liu, R.M.K. Carlson, Science 299 (2003) 96.
[5] H. Schwertfeger, A.A. Fokin, P.R. Schreiner, Angew. Chem. Int. Ed. 47 (2008) 1022.
[6] A.T. Balaban, P. von Ragué Schleyer, Tetrahedron 34 (1978) 3599.
[7] W. Burns, M.A. McKervey, T.R.B. Mitchell, J.J. Rooney, J. Am. Chem. Soc. 100 (1978) 906.
[8] F.J. Himpsel, J.A. Knapp, J.A. VanVechten, D.E. Eastman, Phys. Rev. B 20 (1979) 624.
[9] J. Van der Weide, R.J. Nemanich, Appl. Phys. Lett. 62 (1993) 1878.
[10] C. Bandis, B.B. Pate, Phys. Rev. Lett. 74 (1995) 777.
[11] J.B. Cui, J. Ristein, L. Ley, Phys. Rev. B 60 (1999) 16135.
[12] D. Takeuchi et al., Appl. Phys. Lett. 86 (2005) 152103.
[13] W. Zhu, G.P. Kochanski, S. Jin, Science 282 (1998) 1471.
[14] A. Watanabe, M. Deguchi, M. Kitakatake, S. Kono, Ultramicroscopy 95 (2003) 145.
[15] N.D. Drummond, A.J. Williamson, R.J. Needs, G. Galli, Phys. Rev. Lett. 95 (2005) 096801.
[16] B.A. Tkachenko et al., Org. Lett. 8 (2006) 1767.
[17] T.M. Willey et al., J. Am. Chem. Soc. 130 (2008) 10536.
[18] W.L. Yang et al., Science 316 (2007) 1460.
[19] W.A. Clay et al., Nano Lett. 9 (2009) 57.
[20] Y. Wang et al., Nat. Mater. 7 (2008) 38.
[21] A.A. Fokin, B.A. Tkachenko, P.A. Guchenko, D.V. Gusev, P.R. Schreiner, Chem. Eur. J. 11 (2005) 7091.
[22] A.A. Fokin, P.R. Schreiner, Mol. Phys. 107 (2009) 823.
[23] N.A. Fokina et al., Eur. J. Org. Chem. (2007) 4738.
[24] R.M. Petoral Jr., K. Uvdal, J. Electron. Spectrosc. Relat. Phenom. 128 (2003) 159.
[25] G.E. Poirier, E.D. Pylant, Science 272 (1996) 1145.
[26] A. Ulman, Chem. Rev. 96 (1996) 1533.
[27] M. Muntwiler, M. Hengsberger, A. Dolocan, H.J. Neff, T. Greber, J. Osterwalder, Phys. Rev. B 75 (2007) 075407.
[28] M.K. Reed, M.K. Steiner-Sheppard, D.K. Negus, Opt. Lett. 19 (1994) 1855.
[29] T. Greber, O. Raetzo, T.J. Kreutz, P. Schwaller, W. Deichmann, E. Wetli, J. Osterwalder, Rev. Sci. Instrum. 68 (1997) 4549.
[30] T. Sasagawa, Z.-X. Shen, J. Appl. Phys. 104 (2008) 073704.
[31] P.C. Rusu, G. Brocks, Phys. Rev. B 74 (2006) 073414.
[32] The absorbance of the sample surface is calculated using the bulk optical constants for silver; the reflectance at 30° light incidence is 91% and 99% for 400 and 800 nm light, respectively.
[33] H. Eckardt, L. Fritsche, J. Noffke, J. Phys. F: Met. Phys. 14 (1984) 97.
[34] M. Aeschlimann, M. Bauer, S. Pawlik, Chem. Phys. 205 (1996) 127.
[35] R. Keyling, W.-D. Schöne, W. Ekardt, Phys. Rev. B 61 (2000) 1670.
[36] V.P. Zhukov, F. Aryasetiawan, E.V. Chulkov, I.G. de Gurtubay, P.M. Echenique, Phys. Rev. B 64 (2001) 195122.
[37] E. Knoesel, A. Hotzel, M. Wolf, Phys. Rev. B 57 (1998) 12812.
[38] M. Drescher et al., Nature 419 (2002) 803.
[39] L. Miaja-Avila, C. Lei, M. Aeschlimann, J.L. Gland, M.M. Murnane, H.C. Kapteyn, G. Saathoff, Phys. Rev. Lett. 97 (2006) 113604.
[40] S. Passlack, S. Mathias, O. Andreyev, D. Mittnacht, M. Aeschlimann, M. Bauer, J. Appl. Phys. 100 (2006) 024912.
[41] J. Graf et al., J. Appl. Phys. 107 (2010) 014912.
[42] M. Rohleder, W. Berthold, J. Güdde, U. Höfer, Phys. Rev. Lett. 94 (2005) 017401.
[43] W.F. Krolikowski, W.E. Spicer, Phys. Rev. B 1 (1970) 478.